2024

UNDERWATER VEHICLE MANEUVERING WITH A SINGLEBLADED PROPELLER

Benjamin C. S. Rahming
University of Rhode Island, brahming@uri.edu

UNDERWATER VEHICLE MANEUVERING WITH A SINGLE BLADED PROPELLER

BY

BENJAMIN C. S. RAHMING

A THESIS SUBMITTED IN PARTIAL FULFILLMENT OF THE

REQUIREMENTS FOR THE DEGREE OF

MASTER OF SCIENCE

IN

OCEAN ENGINEERING

UNIVERSITY OF RHODE ISLAND

2024

MASTER OF SCIENCE THESIS

OF

BENJAMIN C. S. RAHMING

APPROVED:

Thesis Committee:

Major Professor Stephen Licht
Jason Dahl
Musa Jouaneh
Brenton DeBoef

DEAN OF THE GRADUATE SCHOOL

UNIVERSITY OF RHODE ISLAND

2024

ABSTRACT

Current convention in underwater vehicle propulsion utilizes a symmetrical propeller with fins or additional thrusters for maneuvering. These systems can become mechanically and electronically complex requiring multiple sensors and actuators such as motors, motor controllers, encoders and water tight seals. This creates many failure modes. Conversely, an asymmetrical propeller has fewer failure modes as the propeller can maneuver the vehicle by itself. By varying the speed of the blade within the rotation, the resulting force imbalance creates a turning moment in addition to forward thrust. This thesis designs, develops and utilizes a test bed to decipher the six axis dynamic capabilities of a single bladed asymmetrical propeller.

ACKNOWLEDGMENTS

I would like to thank my advisor, Dr. Stephen Licht, for his knowledge and guidance, my lab mates for the their assistance, Ervin for his consistent support and conversation, my parents, Bernard and Carmen, my brother, Bernard my family and my partner, Jennifer, for their love. Most of all, I would like to thank my creator.

I dedicate this work to my grandfathers, Clayman Butts and Samuel Rahming.

TABLE OF CONTENTS

Page

LIST OF FIGURES

CHAPTER 1

Introduction

A single bladed propeller can provide full actuation using a single rotary actuator with fewer failure modes and less cost than a platform with controls surfaces or additional thrusters. Using a single bladed propeller removes the need for additional actuators used for maneuvering. A cheaper, more reliable alternative opens ocean exploration to researchers who may not have the funding to afford an underwater vehicle. A vehicle will less failure modes can explore deeper depths on a smaller platform. A smaller vehicle reduces the operation costs by removing the need for a large vessel, a winch or other requirements for deploying a large vehicle in the field.

Although the ocean covers roughly 70% of the earth's surface, modern scientists have observed less than 20% of the marine environment [1]. Part of this lack of exploration results from the high costs associated with oceanic expeditions and vehicles. At the University of Rhode Island, the Robotics Laboratory for Complex Underwater Environments (RCUE) and the Undersea Robotics and Imaging Lab (URIL) develop novel vehicles and imaging platforms with the goal of creating lower cost maritime instrumentation [2,3,4,5].

This project aims to develop an alternative propulsion and control system for remote operated vehicles (ROVs) and autonomous underwater vehicles (AUVs) that reduces cost by reducing complexity. ROVs are typically used for precise surveys and sampling, as they can hold their place [8]. AUVs are often used for large scale surveys and sampling, due to their freedom from tether [7]. ROV maneuvering is typically achieved using multiple propeller thrusters [8]. This allows for more station keeping and hovering [7]. AUV maneuverability is traditionally

achieved with forward thrust from a propeller and turning moment from control surfaces(i.e. fins), or with a single azimuthing thruster [8]. This requires an AUV to consistently move forward to maintain depth and heading control [8].

1.1 Background

This effort is a direct follow to previous work with single bladed propulsion by Robert Carelli [9] and Kaeli et al. [8]. Carelli discovered that the single bladed propeller could achieve a higher maximum propulsion efficiency than a symmetrical two bladed propeller in open water for some operating points relevant to AUV operations. Figure 1, adopted from Carelli [9], provides an example case for physical performance. Carelli looked at a case when the two bladed propeller generated a thrust equivalent to $K_t = 0.11$, represented by the horizontal red line. This thrust value corresponds to an advance ratio of 0.40, represented by the vertical orange line. Carelli calulated that the single bladed propeller would require an advance ratio of 0.36 to match the operating point of the two bladed propeller in this scenario.Although the single blade needed a 10% higher RPM, the result was a 12% higher efficiency.

Carelli also demonstrated the single bladed propeller had the ability to generate torque through tow tank trials. Figure 2 depicts Carelli's experimental setup. Carelli concluded the thesis with three recommendations for future research; testing the steering effectiveness of a single bladed propeller against a traditional propeller with control fins; testing an asymmetrical propeller with multiple blades; and development of a free swimming vehicle that utilizes asymmetrical propulsion to identify operational constraints and practical considerations for this novel method of propulsion [9].

Kaeli et al. continued asymmetrical propulsion research by developing a platform that utilizes a single bladed propeller, addressing the recommendation

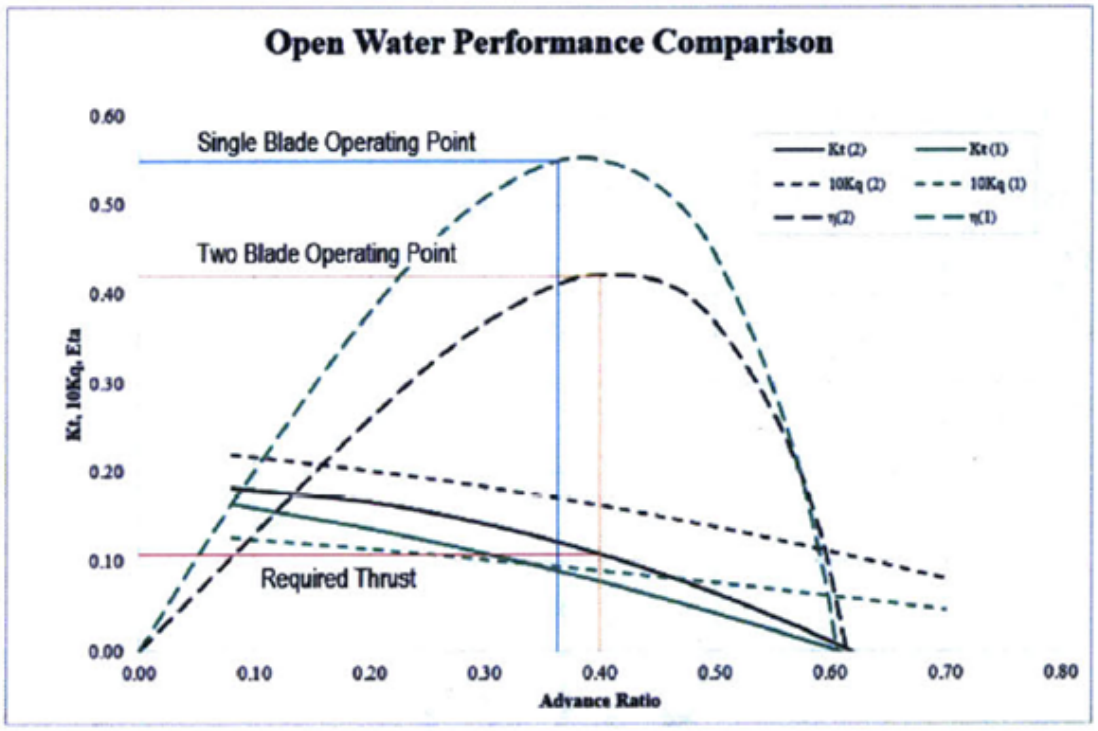

Figure 1. Carelli compares open trials of single blade against two blade, advance ratio on the x axis, non dimensional coefficients for thrust, Kt, and torque, Kq, as well as efficiency, on the y axis [9]

for future research. Kaeli et al. found that operating at a higher RPM with smaller RPM changes for steering is more effective than the opposing situation, operating at a slower RPM with larger changes in RPM. The team designed, fabricated and tested the vehicle. Figure 3, below demonstrates the platform's ability to turn starboard (middle) and port (bottom) [8]. Figure 4, demonstrates the ability to maintain station in a tank setting using alternating forwards and backwards to turn [8]. Kaeli et al. also tested the vehicle in open water [8].

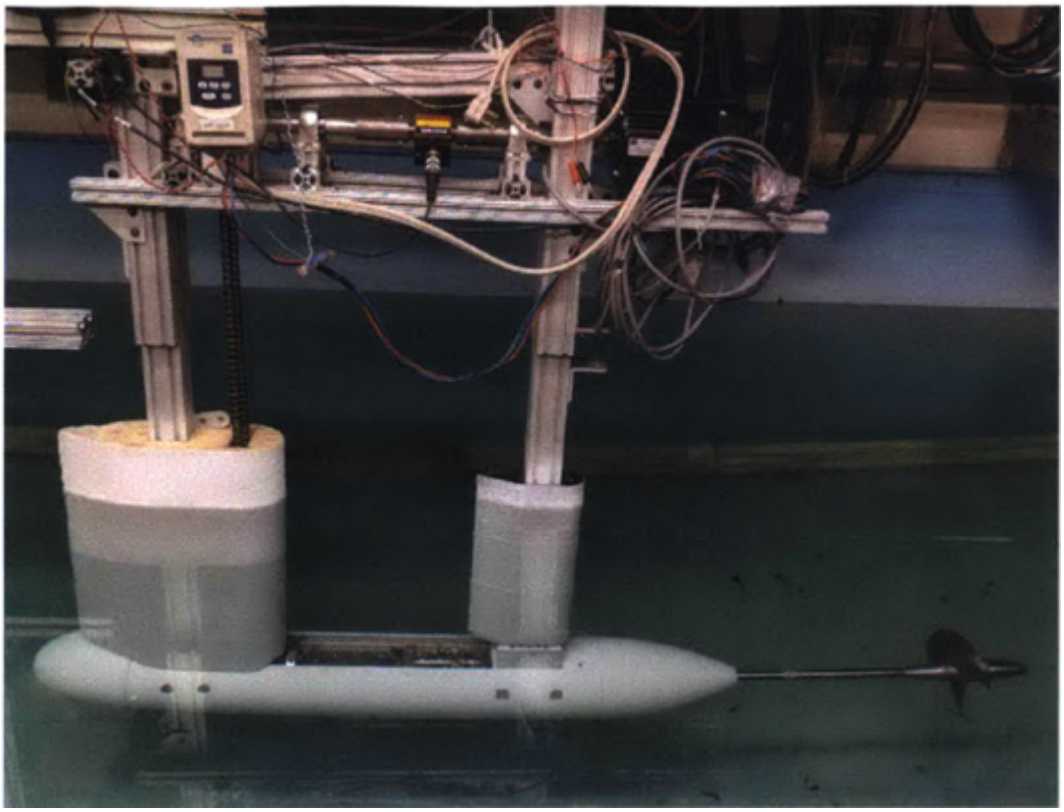

Figure 2. Carelli's tow tank apparatus [9]

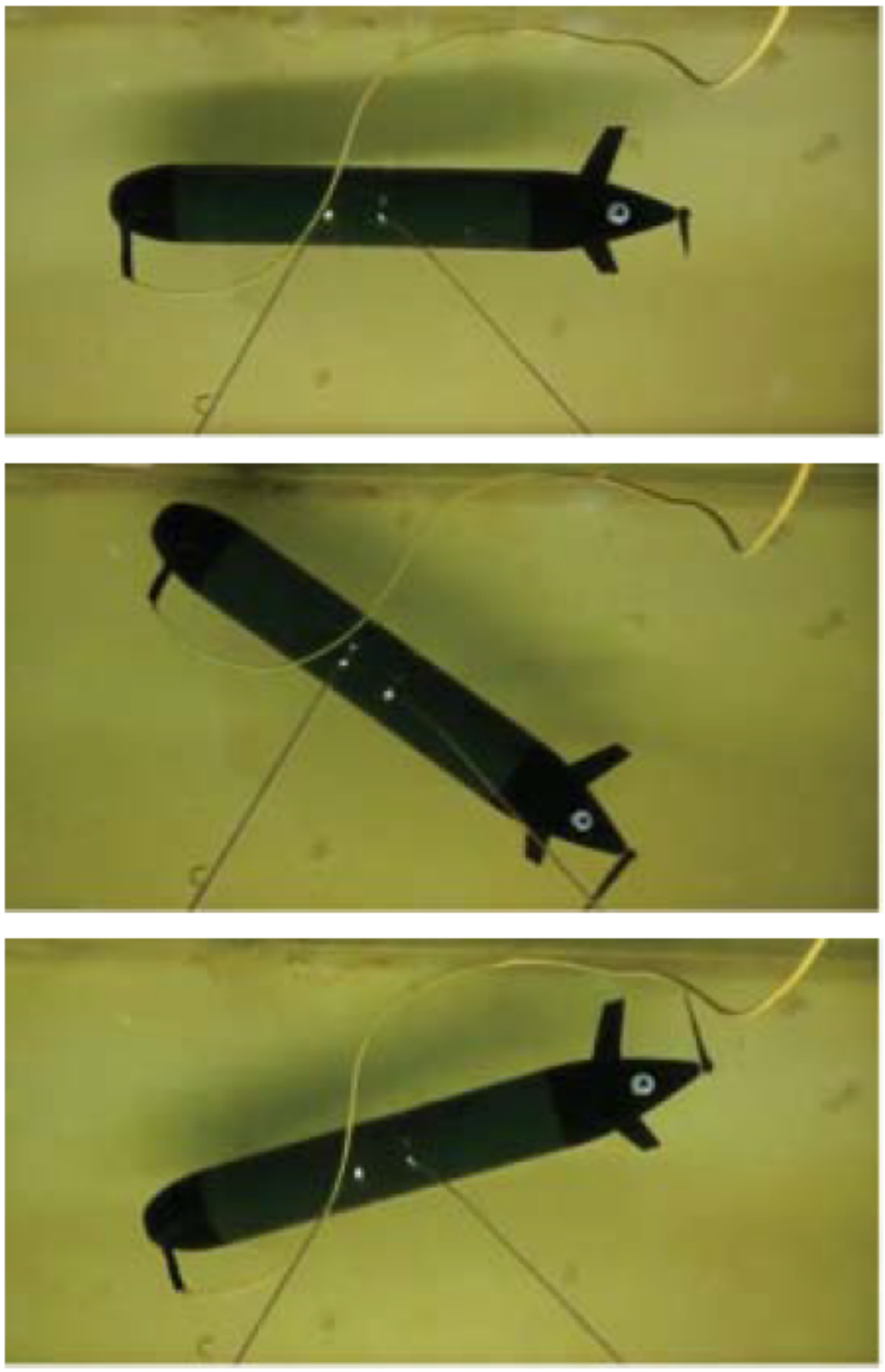

Figure 3. Littlefield et al. tank testing with the vehicle at rest (top), turning to starboard (middle), and turning to port (bottom) while controlled via tether [8]

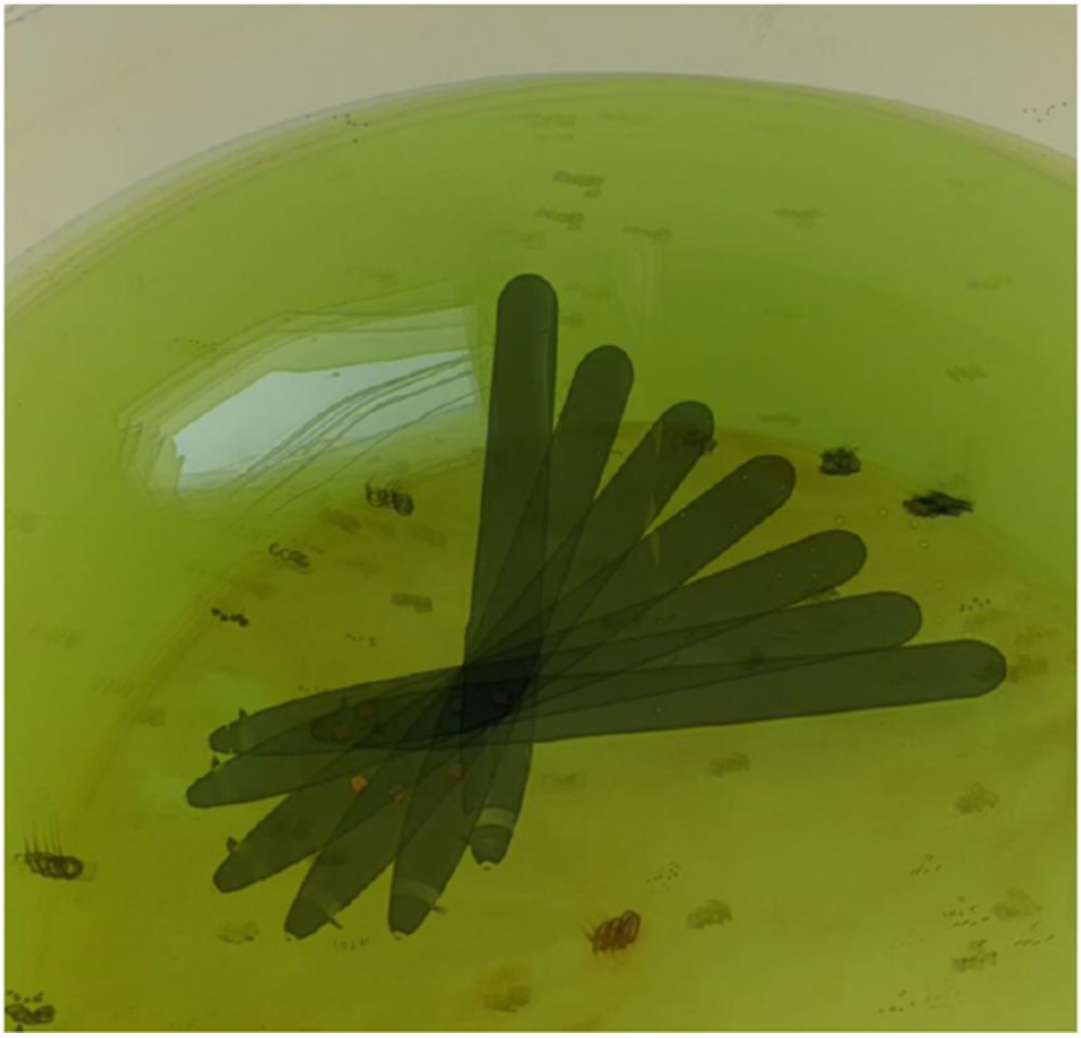

Figure 4. Littlefield et al. tank testing with the vehicle at rest (top), turning to starboard (middle), and turning to port (bottom) while controlled via tether [8]

Carelli gathered dynamometry data of an asymmetrical propeller by itself. Kaeli et al., developed a vehicle around asymmetrical propulsion technology. Through developing an experimental setup and process, the goal is to build a quantitative understanding of the asymmetrical propeller's dynamic capabilities when propelling a vehicle. The goal of this thesis is to relate changes in RPM to generated maneuvering torques. In short, this thesis builds a validated test bed to combine dynamometry, propeller angular position and instantaneous RPM, with future simultaneous wake visualization.

CHAPTER 2

Methods

A test bed was created capable of measuring force as a function of propeller angular trajectory for an asymmetric propeller mounted to a vehicle hull. The experimental design criteria included support for future wake flow visualization synced to propeller position and dynamometry data collection. However, wake flow visualization was not performed in this present study. The experimental test bed was constructed using a prototype vehicle tail section provided by ARMADA Marine Robotics [Woods Hole, MA] in a recirculating flume tank at the University of Rhode Island [Narragansett, RI] shown in Figure 11.

2.1 Vehicle Prototype

The platform consists of drive electronics for a single bladed propeller in a cylindrical pressure housing, with a drive shaft extending from the tail section with a shroud. The cylinder has a diameter of 12.7 cm and length of 62.2 cm.

The propeller blade used in this experiment has a span of 4.45 cm and a 23° pitch angle. At the base the chord is 2.03 cm, the chord is 2.92 cm span at maximum and 2.74 cm at the tip. The blade is 0.30 cm thick and 4.3 cm long. The hub tapers from fore to aft from a diameter of 3.56 cm to a diameter of 1.91 cm. The dimensions of the shroud are shown in Figure 7. Shroud diameter averages 11.9 cm, with maximum thickness 4.9 cm, and cord length 4 cm. The propeller was 3D printed in ABS.

The propeller is driven by a three phase brushless DC motor. A PIC32MK microcontroller unit (MCU) [32-Bit, 120 MHz performance with 1MB of Flash memory] with an embedded quadrature encoder module is used for motor con-

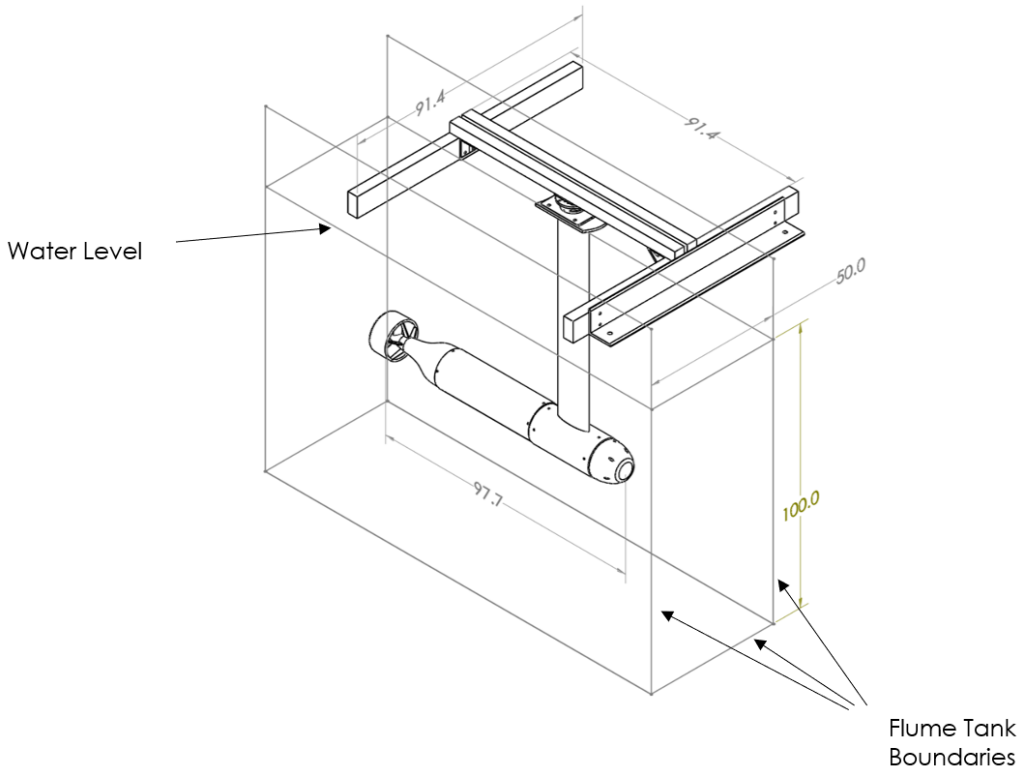

Figure 5. Isometric view of vehicle mounted to frame, dimensions in cm

trol [8]. The system uses the embedded encoder in conjunction with an external magnetic encoder to sense the shaft position and instantaneous velocity with a time resolution of approximately 5 µs [8].

Mean revolutions per minute [RPM] ranged from 844-925 for tests at 0.25 m/s flow speed and 2429-2600 for tests at 0.60 m/s flow speed. Pulse width modulation [PWM] motorspeed control was used to command the propeller drive motor and hence propeller RPM. For the propeller position in the body frame, 0° corresponds to the propeller pointing up, 90° to port, 180° to down and 270° to starboard. Maneuvering torque was commanded as a magnitude and direction. This geometry means that when generating a maneuvering torque down the RPM peaks at 0° to steer the vehicle towards 180°. Figure 8 shows instantaneous RPM, as a function of θ, angular position of propeller blade for a case

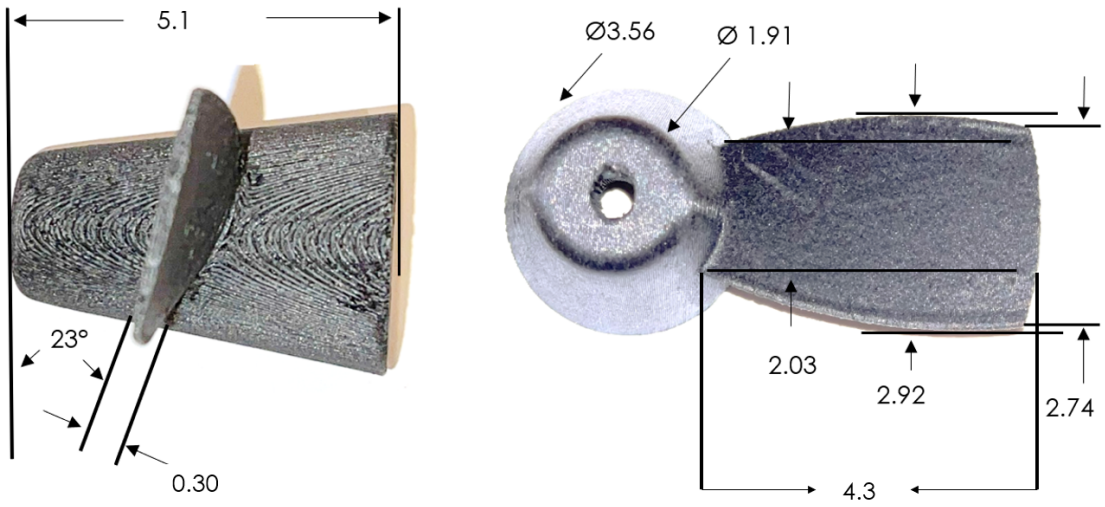

Figure 6. Side view (left) and top view (right) of single bladed propeller provided by ARMADA Marine Robotics, dimensions in cm

where the steering angle recommended is 180°.

Mean RPM and actual RPM were measured by an encoder built into the system. Actual RPM gives 18 counter values at 20° increments. The propeller commands were input from a separate laptop via a RS-232 serial connection, managed in a Realterm terminal window, version 2.0.0.69, under Windows 11. Both the sensor and the vehicle were powered from separate power supplies.

2.2 Recirculating Flume

The vehicle prototype is mounted in a recirculating flume with controllable flow speeds up to 1.0 m/s. The flume has dimensions of 50 cm width, a water depth maintained at 100 cm and 818 cm usable length. The front of the prototype tail section was attached to a circular plate. This circular plate was attached perpendicularly to a rectangular custom mating plate [Figure 10], which was attached to another circular plate. A 3D printed [PLA, Prusa] nose cone, designed by ARMADA, was then attached to the front circular plate. A fairing was placed over the vehicle mounting section. The power and communication wiring for the

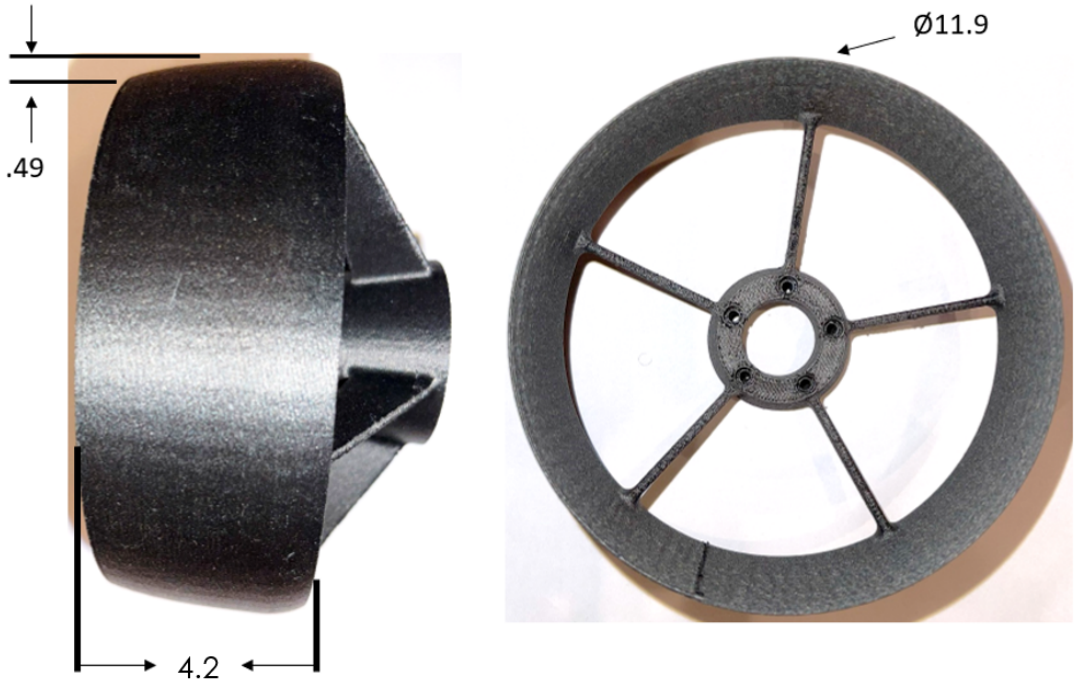

Figure 7. Back view(left) and side view(right) of shroud provided by ARMADA Marine Robotics, dimensions in cm

vehicle prototype was routed through the center of the hollow mast which consisted of aluminum originally designed for recreational foil boarding [Axis]. The fairing and the wiring were intended to disturb the flow as little as possible.

Dynamometry data was collected using an ATI Gamma F/T Sensor SI-130-10. The vehicle was attached to the force torque sensor with an 820 mm aluminum mast. The force sensor was connected to a frame of 80/20 beams using additional custom mating plates. The 80/20 frame was bolted to L-beams that were bolted to the top of the tank. The ATI Gamma sensor analog output channels were connected to the differential inputs of a 16 bit data acquisition module [National Instruments, NI DAQ USB-6212].

The apparatus frame was primarily built with 80/20 aluminum t-slotted framing rails. In Figures 5 and 9, these rails are pictured as rectangular prisms for clarity. The central axis of the vehicle was held at a water depth of 57.7 cm when

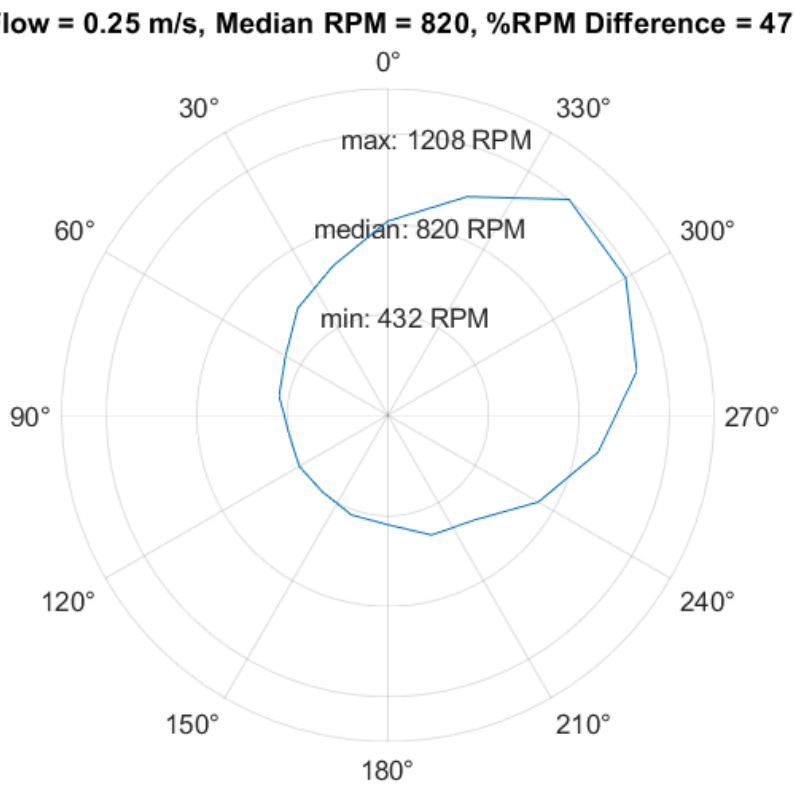

Figure 8. Polar plot of propeller generating maneuvering torque down with 47% RPM Difference

mounted. The bow of the vehicle was mounted 455 cm downstream from the flume outlet to minimize flow variability.

Experiments were performed with flow speeds at 0.25 m/s and 0.60 m/s. Flow speed data was taken with a laser doppler velocimetry (LDV) sensor built by Measurement Science Enterprise, Inc. At 0.25 m/s, the root mean square (RMS) error was 0.031 m/s with a mean signal to noise ratio (SNR) of 4.53 after 2,724 samples. At 0.60 m/s, the RMS error was 0.09 m/s with a mean SNR of 3.14 after 2,122 samples.

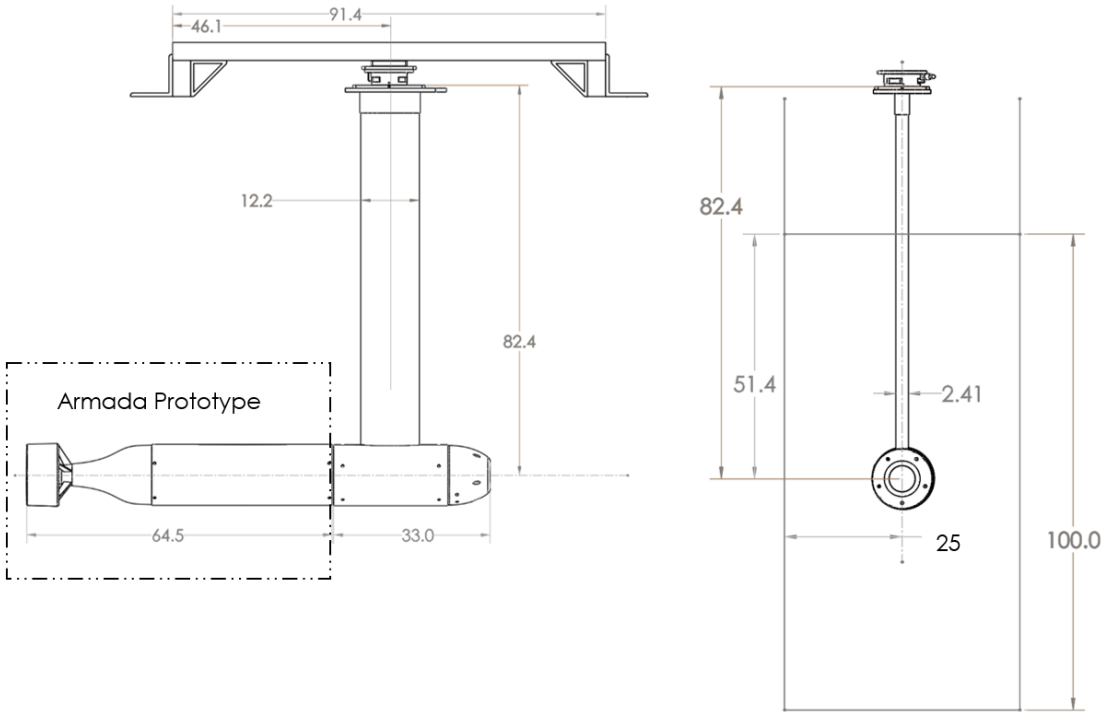

Figure 9. Side view of apparatus (left) front view without frame (right), dimensions in cm

2.3 Control and Sensing

Experimentally controlled variables during recorded trials were, dynamometry data acquisition (DAQ) rate, trial length, propeller drive command mean pulse width modulation (PWM) frequency and duty cycle, maneuvering torque angle, maneuvering torque amplitude and tank flow speed percentage. Vehicle voltage, DAQ rate and trial length were held constant throughout the experiment. Voltage was controlled by an external power supply held at 7 V. The DAQ rate at 1100 HZ, and trial length at 2 minutes were set within the MATLAB data collection script. MATLAB version R2023b was used with the Data Acquisition Toolbox. Trials ran at two flow speeds, 0.25 m/s and 0.60 m/s. Figure 11 shows the flow traveled bow to stern, the negative x direction in the body frame. For each flow speed, sample trials were run to determine the mean propeller RPM that resulted in a net zero force in the x direction with no maneuvering torque

input.

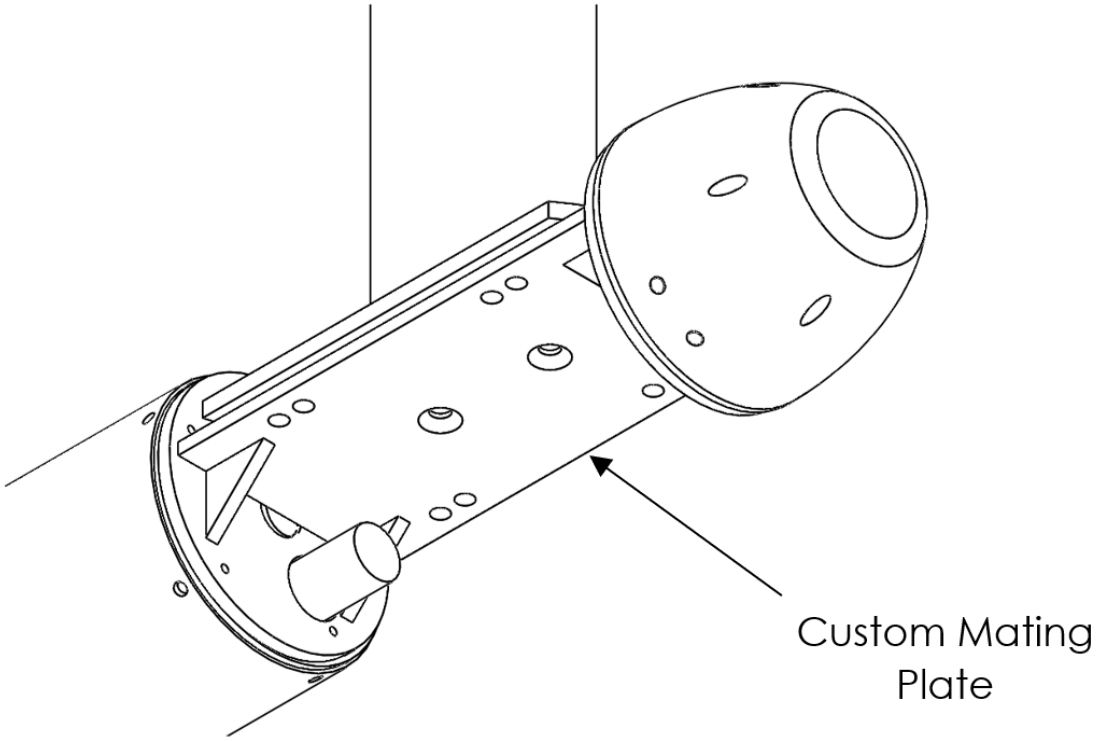

Figure 10. Apparatus close up without fairing showcasing custom mating plate

2.4 Test Procedure

Throughout the experiment, the position of the vehicle remained fixed, while water in the flume tank flowed from bow to stern. A laser doppler velocimetry sensor was used to gather flow speed data 46 cm in front of the nose cone. Prior to each trial, dynamometry data was collected with no flow and no propeller thrust for two minutes. As the strain gauges in the force torque sensor will always return some level of voltages, this data set serves as the zero bias for the following data sets. Data sets were then collected with nominal flow speeds at 0.25 m/s and 0.60 m/s, and no propeller actuation to measure the drag force on the vehicle. The speed of the propeller was then increased to generate thrust equivalent and opposite the drag force. To find a change in load, the zero bias is

subtracted from signals with thrust. The resulting change in voltage is converted into force, [N], and torque, [N-m] using a validated calibration matrix supplied by ATI.

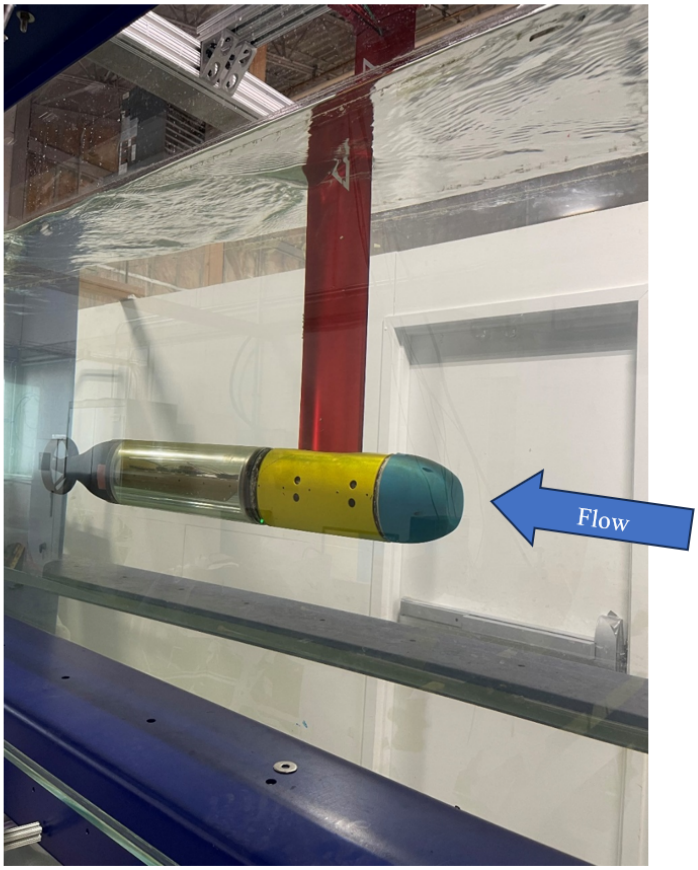

Figure 11. Apparatus in flume tank

The force and torque signals are then low pass filtered to remove high frequency components resulting from interactions between flow variability and the apparatus resonant frequency. A low pass infinite impulse response filter [IIR] of order three, with a passband frequency of 1 Hz, a passband ripple of 1 Hz and a sample rate of 1100 Hz, was used to remove high frequency flume and electronic noise from the dynamometry data.

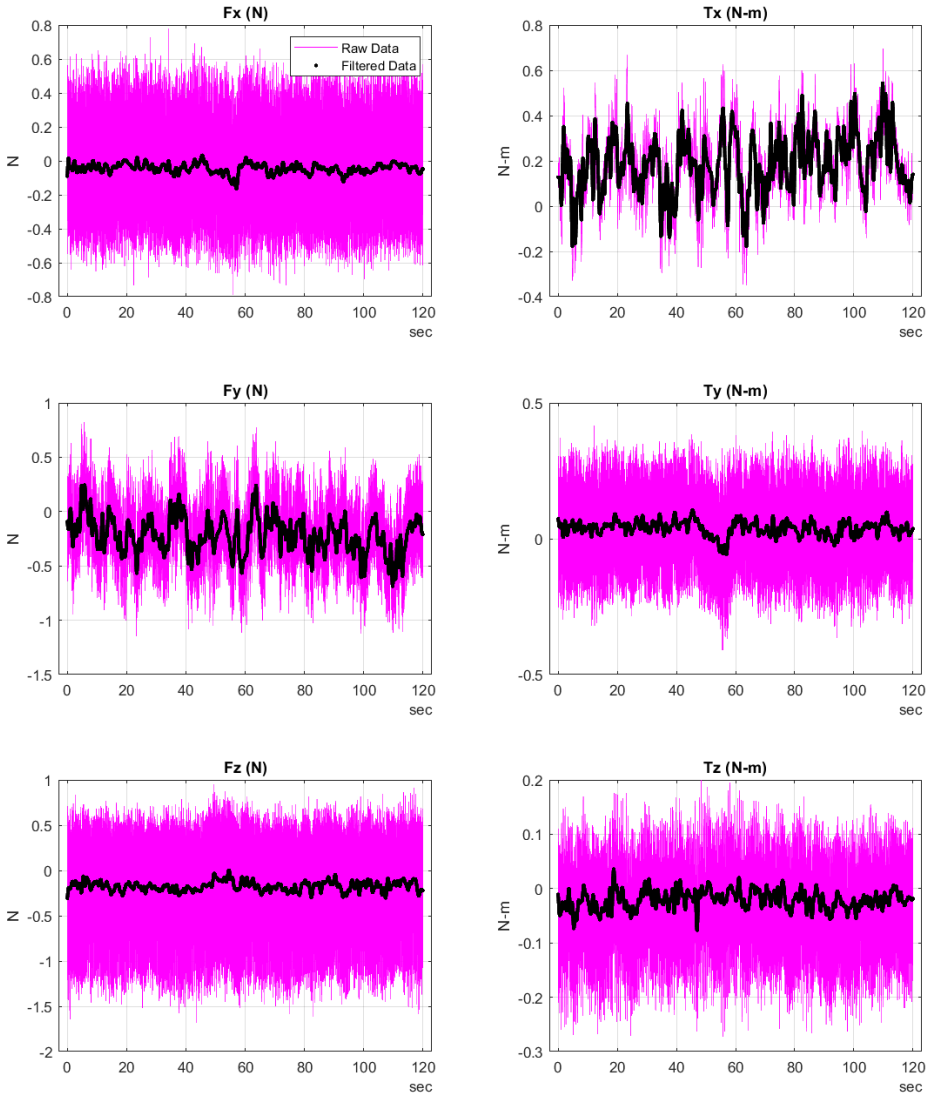

Figure 12. Raw data shown with filter, generating maneuvering torque to pitch down at 47% RPM delta

The dynamometry sensor utilizes strain gauges to convert force and torque measurements into voltage signals. The sensor can also pick up voltage signals from the power supply and mistake these signals as force and torque data. Further, fluctuations from the flow can create alterations in the force and torque

data. Since both of these factors are changing more rapidly than the vehicle dynamics, occurring at a higher frequency, a low pass filter removes these higher frequency components to leave the low frequency vehicle dynamics. Figure 12 shows the raw dynamometry data in magenta with the filtered data in black. For each flow speed, 0.25 and 0.60 m/s, the RPM required to overcome vehicle drag was determined by increasing RPM until the net force on the vehicle (drag + propeller thrust) was found to be zero. The vehicle ran at 7 V and 20% pulse width modulation (PWM) against a nominal flow speed of .25 m/s. At a nominal flow speed of .60 m/s, the vehicle ran at 7V with a PWM percentage of 25. To input a desired direction for maneuvering torque and magnitude, the controller takes steering amplitude percentage and direction. Data was taken for amplitude percentages of 13%,10%,7%,4% and 0%. (A 0% steering input represents the vehicle driving straight.) Maneuvering torque data was taken for steering directions corresponding to port, starboard, nose up and nose down. Figure 8 shows the variability in the instantaneous RPM with an input of 13% amplitude steering nose downward. Figure 13 shows the angle of the blade in degrees on the horizontal axis and the angular velocity in RPM on the vertical axis. The mean RPM is represented by the red line.

Figure 8 showcases the same data in polar coordinates. The angular velocity in RPM is represented by the length of rho or r. Ten separate data points for RPM measurements were taken and averaged for increased accuracy. The propeller dynamics were output from the vehicle prototype processor separated into eighteen 20° intervals. Each interval had a value of counts to represent time spent in that 20° interval. Along with the mean RPM, each 20° interval was averaged with the other values of the same location.

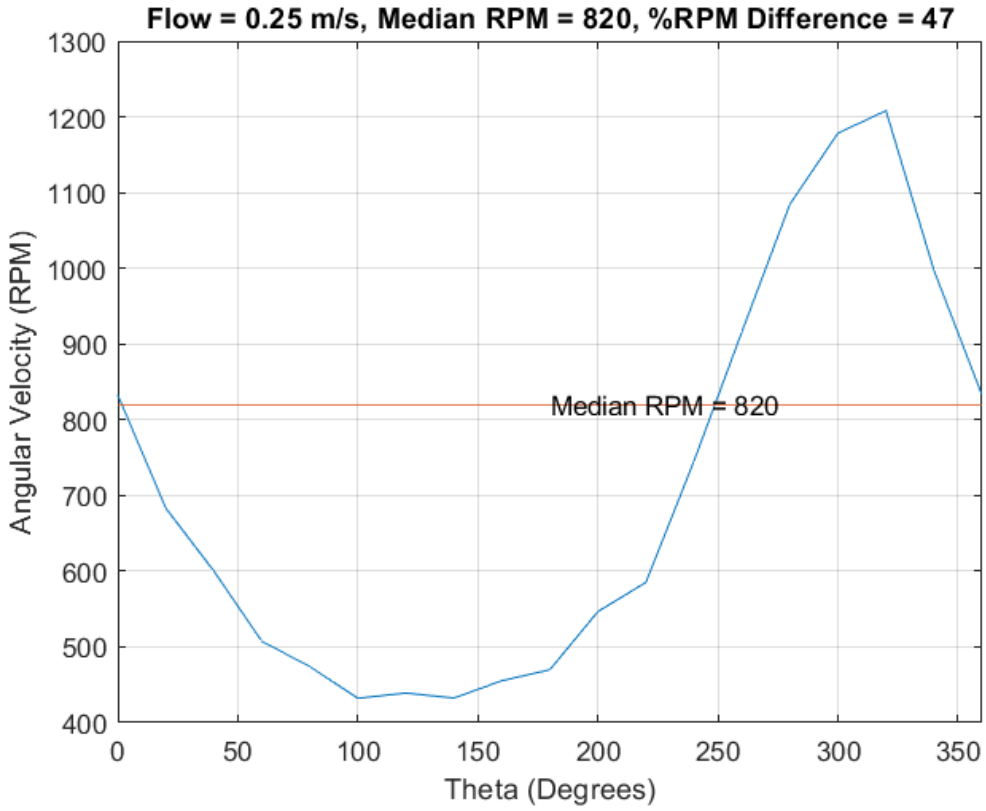

Figure 13. Cartesian plot of propeller generating maneuvering torque down at 47% RPM Difference

2.5 Transformation from Sensor to Body-Fixed Vehicle Reference Frame

As shown in Figure 14, for the vehicle reference frame, the bow is positioned at positive x, the stern at negative x, port at positive y, starboard at negative y, down at positive z and up at negative z. In the body frame, the flow runs in the negative x direction from bow to stern. The sensor reference frame has z downwards as well, with positive y in the port direction and positive x in the stern direction. The data is presented with respect to the body reference frame. To convert thrust into the body frame, the sensor data was multiplied by negative one to switch signs. Equation 2, shows the calculation for X, the force in the x direction in the body frame:

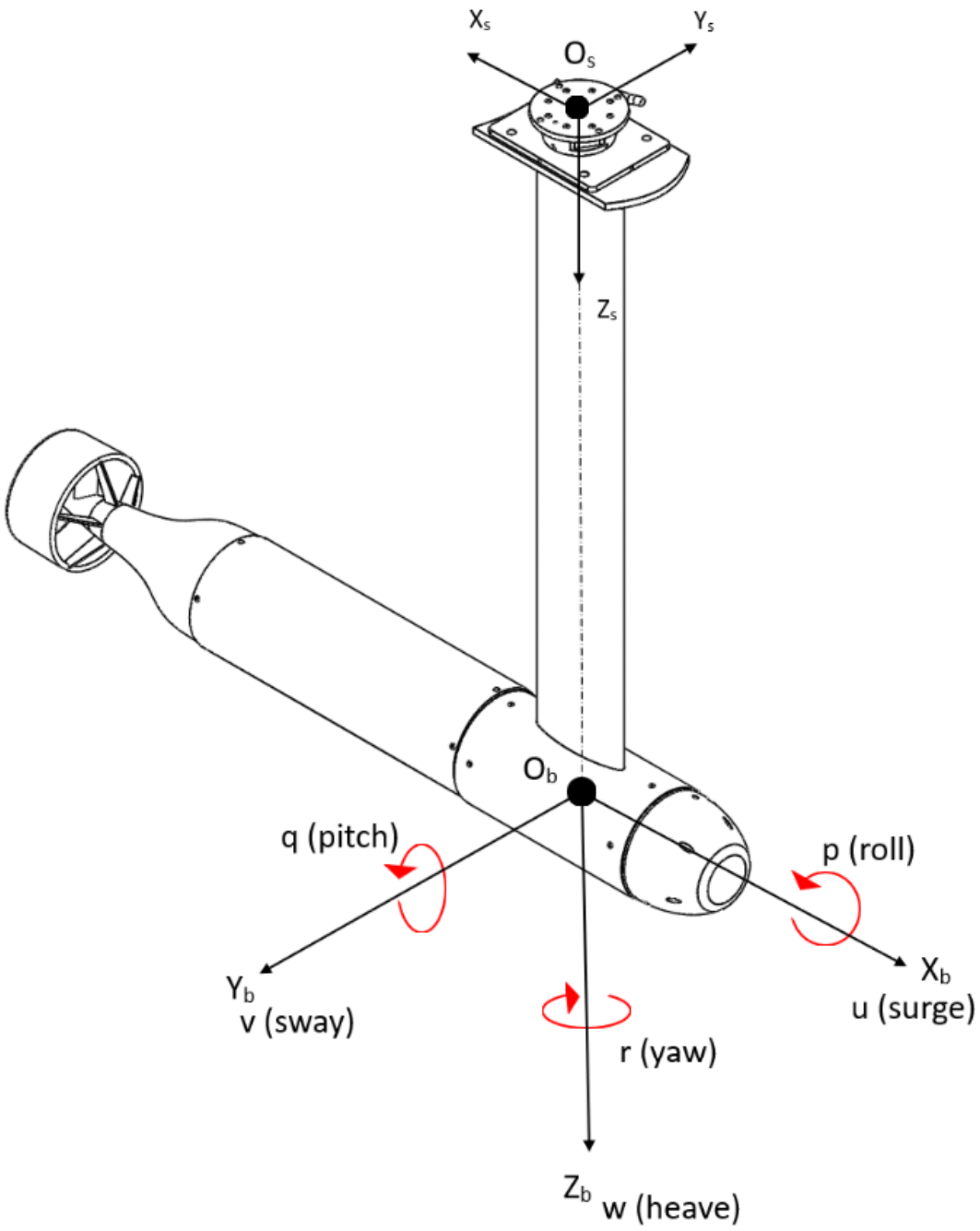

Figure 14. Force diagram on apparatus without frame showing the sensor reference frame and body reference frame

$$x_b = -x_s \tag{1}$$

$$X = -F_{xs} \tag{2}$$

Since the z axes for the body and sensor share direction, no conversion was needed for N , the torque about the z-axis in the body frame:

$$z_b = z_s \tag{3}$$

$$N = -T_{zs} \tag{4}$$

To calculate M, torque about the y-axis in the body frame, the torque about the y-axis in the sensor frame must be multiplied by negative one to change signs. Further, the sensor is also affected by torque generated from any forces in the x-direction acting on the moment arm of the mast. To calculate pitch, the torque from thrust must be removed from Ty. In Figure 15 and equations 5-8, (F_D - F_{px}) represents forces in the x-direction. F_{pz} represents forces generated from the propeller acting in the z-direction, M_p represents a pure moment generated by the propeller:

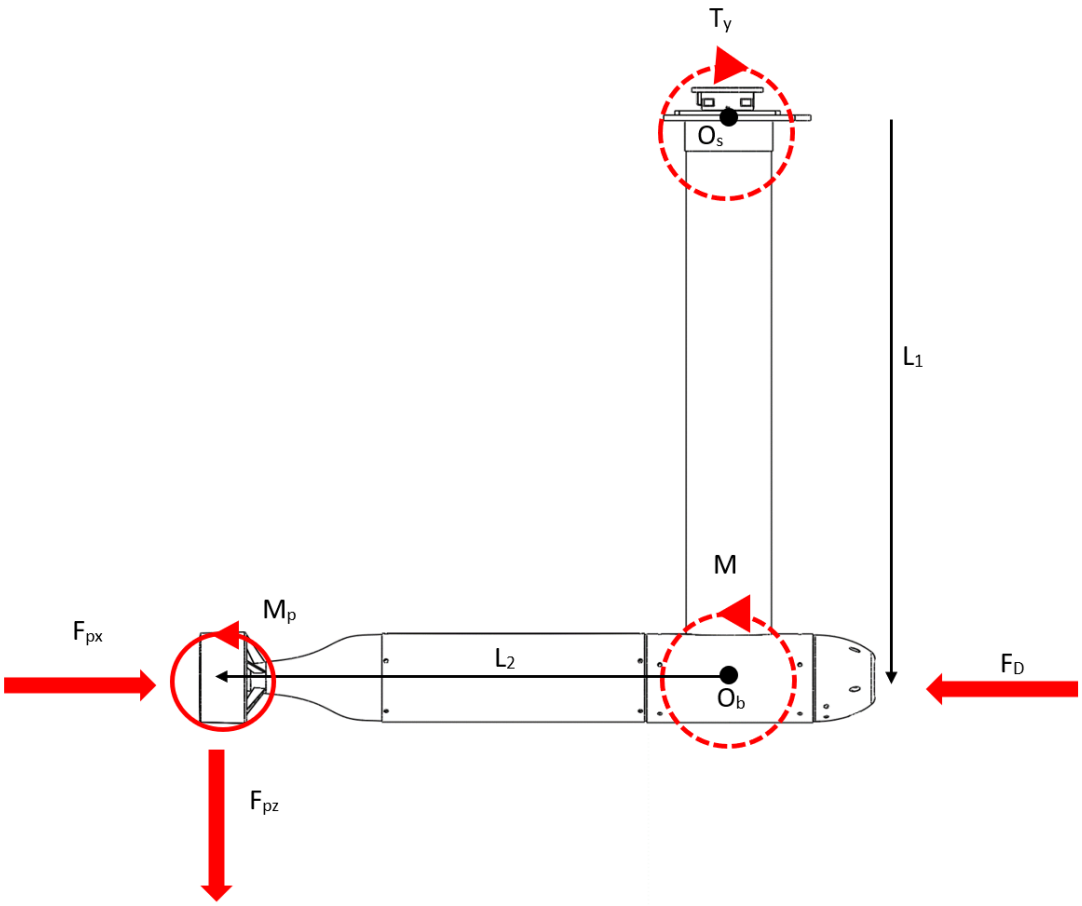

Figure 15. Force diagram from side view, dotted lines signify measured torque

$$T_{ys} = -M_p - F_{pz} * L_2 + (F_D - F_{px}) * L_1 \tag{5}$$

$$M = M_p + F_{pz} * L_2 \tag{6}$$

$$T_{ys} = -M + (F_D - F_{px}) * L_1 \tag{7}$$

$$M = (F_D - F_{px}) * L_1 - T_{ys} \tag{8}$$

CHAPTER 3

Results

Trials were run at two different flow speeds for commanded torques mimicking pure rudder and pure elevator actuation. For each case 10 different torque magnitudes were commanded.

In the rudder actuation trials, experiments ran at 0.25 and 0.60 m/s, with % RPM delta ranging from 0% to 49%, at commanded angles of 270° and 90° for port and starboard respectively.

In Figure 16, the polar plots that showcase the change in RPM within a revolution, the length, ρ , represents the instantaneous RPM and θ represents the position of the propeller blade. Instantaneous RPM values were collected in 20° increments.

The polar figures show the RPM increasing at 220° when generating a maneuvering torque portside and 40° when generating a maneuvering torque starboard side. To match the increase the graphs show a maximum decrease in RPM at 40° when generating a maneuvering torque portside and at 220° when generating a maneuvering torque starboard side. When generating a maneuvering torque port or starboard the data shows an interesting trend with regards to thrust in a flow speed of 0.60 m/s. At an 18% RPM difference the thrust increases, decreases around 30% then increases again around 40% RPM difference.

3.1 Rudder (Yaw Actuation)

In Figure 17, The force and torque data is shown with percent change in RPM on the x-axis. The y-axis shows newtons for thrust and newton-meters for

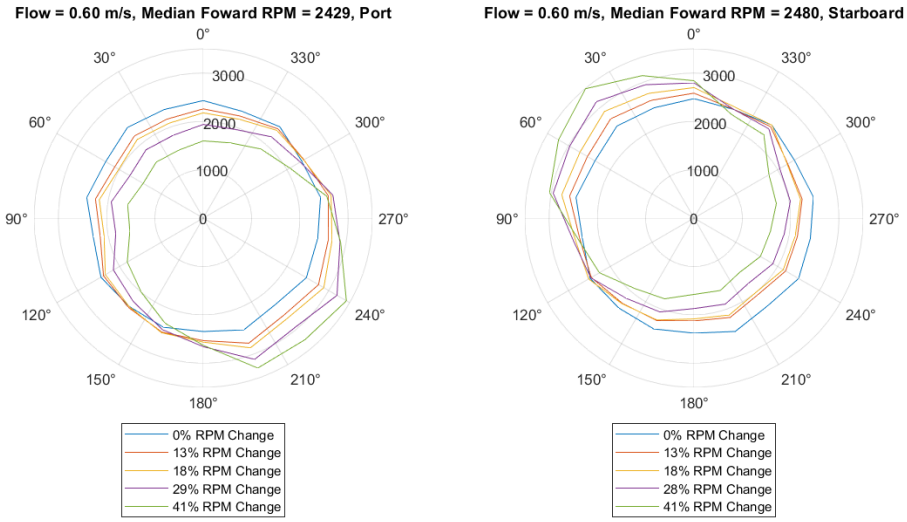

Figure 16. Polar plots of RPM as a function of angular position when generating maneuvering torques port(left) and starboard(right) at flow speed of 0.60 m/s

change in pitch and change in yaw. For thrust, the data is presented unchanged. Both 0% RPM differences port and starboard for rudder; down and up for elevator. When considering rudder change in pitch, and change in yaw graphs are zeroed about the 0% in RPM on the port side. The pitch and yaw value for 0% RPM change starboard is added to the starboard values and removed from the graph. For this reason, the dynamometry graphs are labeled change in pitch and change in yaw as they represent values with respect to a chosen zero.

In yaw, for port to starboard, the results are as expected. With a positive torque in the starboard direction, the data shows a maximum change in torque of 0.45 N-m at 41% RPM Difference. When generating a maneuvering torque port, the data shows -0.43 N-m. The linear regression for change in yaw has a slope of 0.012 (N-M/ % RPM Difference), an intercept of 0.015 N-m and a R^2 value of 0.92.

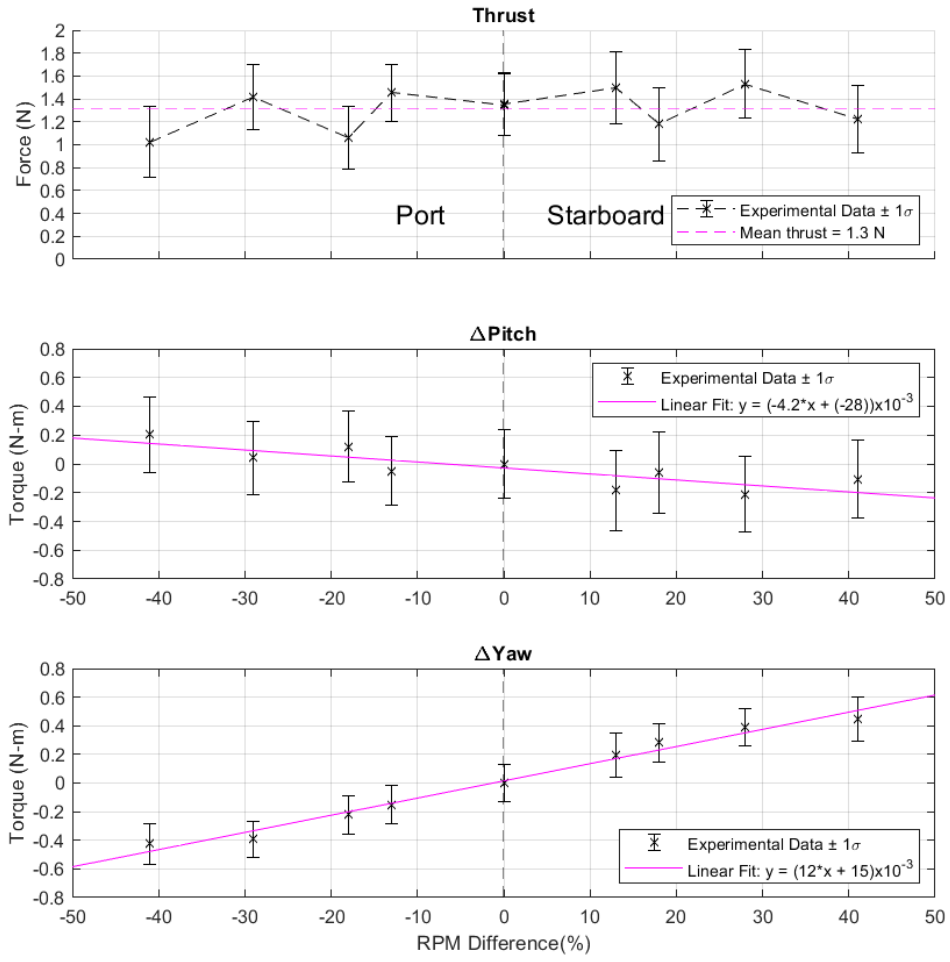

Figure 17. Thrust, change in pitch and change in yaw when generating a maneuvering torque port and starboard at flow speed of 0.60 m/s

For the slower flow speed at 0.25 m/s, maximum RPM change varies slightly at 49% and 48%. Since the propeller rotates slower there is more time for the motor to adjust the angular velocity.

When examining the dynamometry data for the 0.25 m/s flow speed, the thrust when generating a maneuvering torque port has magnitude increases at 49% and 24% RPM changes with respect to 35% RPM change, the data point between them. The thrust when generating a maneuvering torque starboard

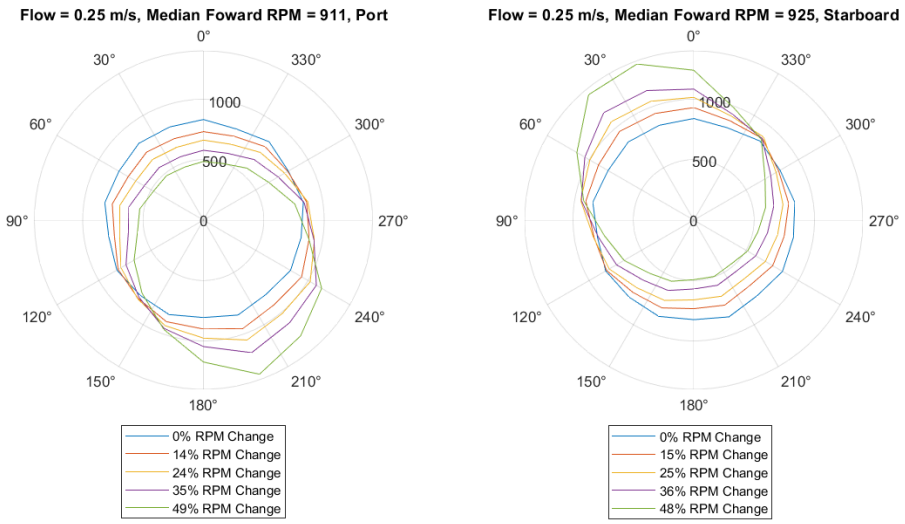

Figure 18. Polar plots of RPM as a function of angular position when generating maneuvering torques port(left) and starboard(right) at flow speed of 0.25 m/s

shows a general decrease from the smallest RPM change, 0%, to the 36% RPM change. There is a minimal increase of .004 N from 36% RPM change to 49% RPM change. Note, however, that the sensor resolution for forces in the x and y directions is .025 N. Since the values are pushing the limits of the sensor resolution and all values within 0.02 it is important to recognize any changes in thrust at 0.25 m/s are minute. The results in yaw when generating a maneuvering torque port or starboard are expected. A positive yaw is clockwise about the positive z-axis, this corresponds to generating a maneuvering torque starboard as seen in the Figure 13. A negative yaw is the opposite, corresponding to generating a maneuvering torque port. The data reflects this geometry. Further, the maximum RPM for the faster, 0.60 m/s, flow speed show a value of -0.41 N-m for port and 0.45 N-m for starboard. These values are only 9% different in magnitude. The yaw results for the 0.25 m/s flow speed show a similar trend, steadily increasing from port to starboard. The maximum RPM difference for the slower, 0.25 m/s, flow speed show a value of -0.042 N-m for port and 0.029 N-m

for starboard. The linear regression for change in yaw has a slope of 0.0008 (N-M/ % RPM Difference), an intercept of 0.0034 N-m and a R^2 value of 0.98.

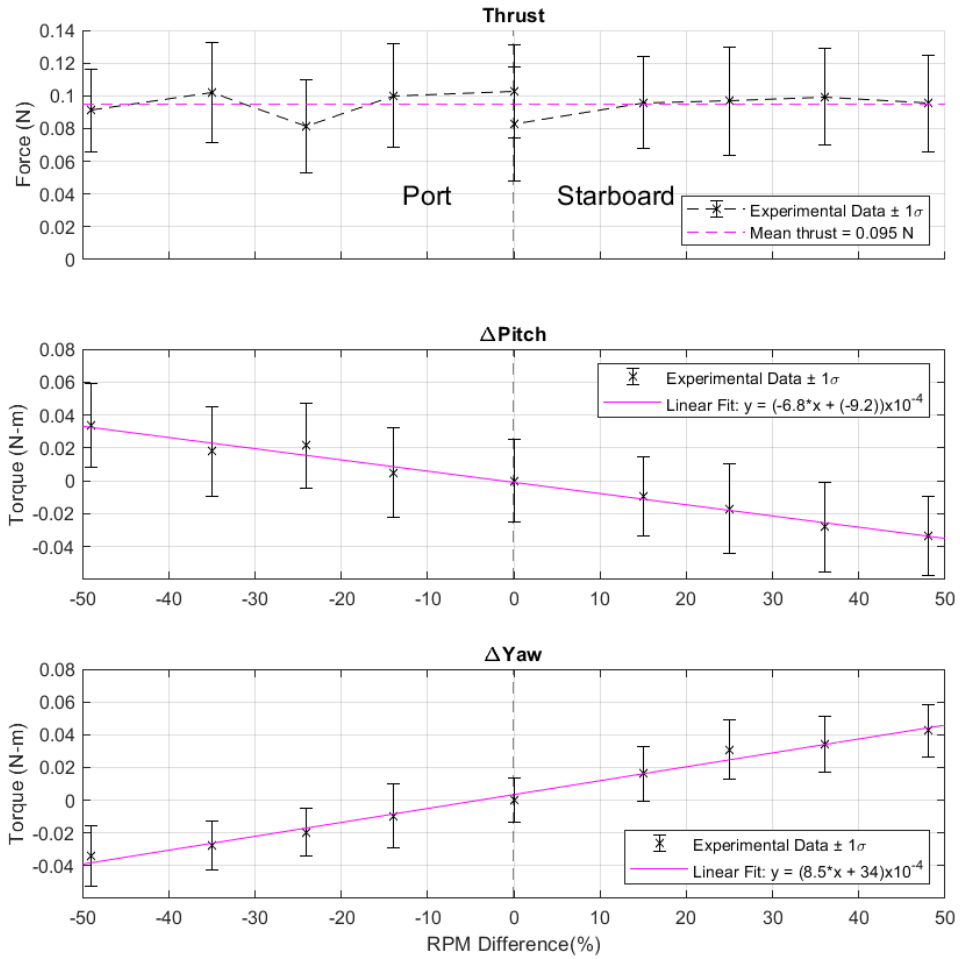

Figure 19. Thrust, change in pitch and change in yaw when generating a maneuvering torque port and starboard at flow speed of 0.25 m/s

3.2 Elevator (Pitch Actuation)

In the elevator actuation trials, experiments ran at 0.25 and 0.60 m/s, with % RPM delta ranging from 0% to 48%, at commanded angles of 270° and 90° for port and starboard respectively. When considering elevator maneuvering torques, the RPM has its maximum increase at 320° and maximum decrease

at 140° elevating down. When generating maneuvering torques down, the maximum RPM increase was at 160° and maximum decrease at 340°.The thrust graph is zeroed about 0% RPM UP.

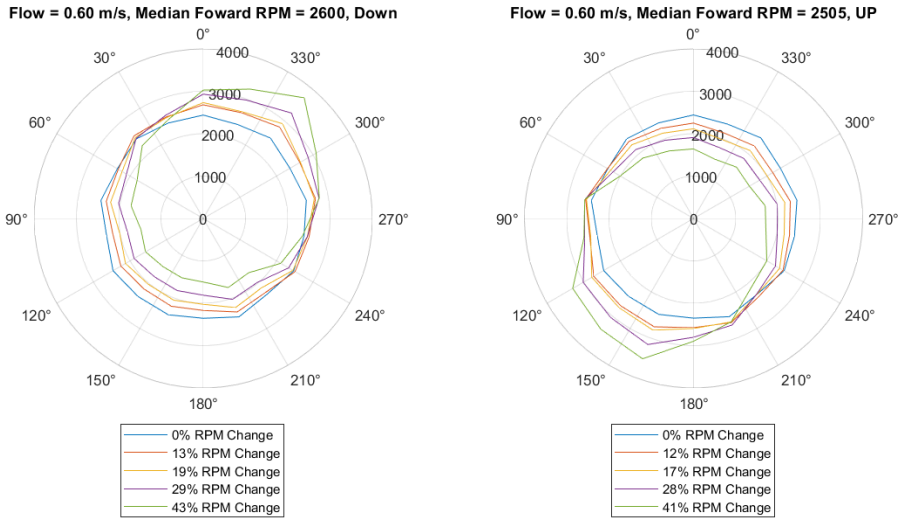

Figure 20. Polar plots of RPM as a function of angular position when generating maneuvering torques down(left) and up(right) at flow speed of 0.60 m/s

The thrust graph shows an unexpected trend for the faster flow speed of 0.60 m/s. 43% RPM difference up has a greater magnitude than 0% RPM difference up. Both the up and down sides of the thrust graph alternate between increasing and decreasing in magnitude. The down side of the thrust graph has a lower magnitude at 41% RPM difference than at 0%. When elevating up and down, pitch or torque about the y-axis is the primary concern. With no propulsion, the vehicle has a positive pitch of 1.09 N-m. At 43% RPM difference elevator up, the pitch is -0.67 N-m and -1.72 N-m at 41% RPM difference elevator down. Though the yaw is not a big concern when elevating, it is important to note that the yaw magnitudes at the maximum RPM differences are -0.099 N-m and 0.062 N-m, for down and up respectively, while the magnitudes for pitch at the maximum RPM differences are -0.42 N-m and .49 N-m, for down and up

respectively. The slope for the linear regression for the change in pitch data is 0.012 (N-M/ % RPM Difference), the y-intercept is -0.014 N-m and the R^2 value is 0.92.

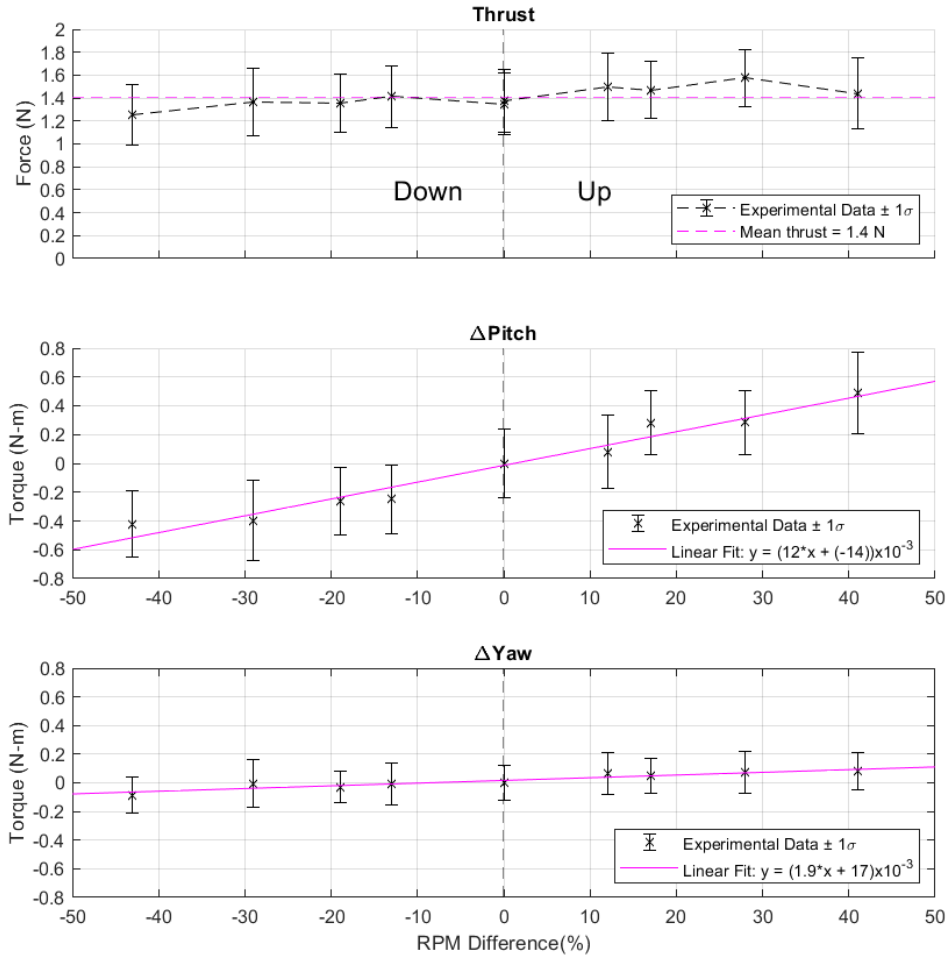

Figure 21. Thrust, change in pitch and change in yaw when generating a maneuvering torque up and down at flow speed of 0.60 m/s

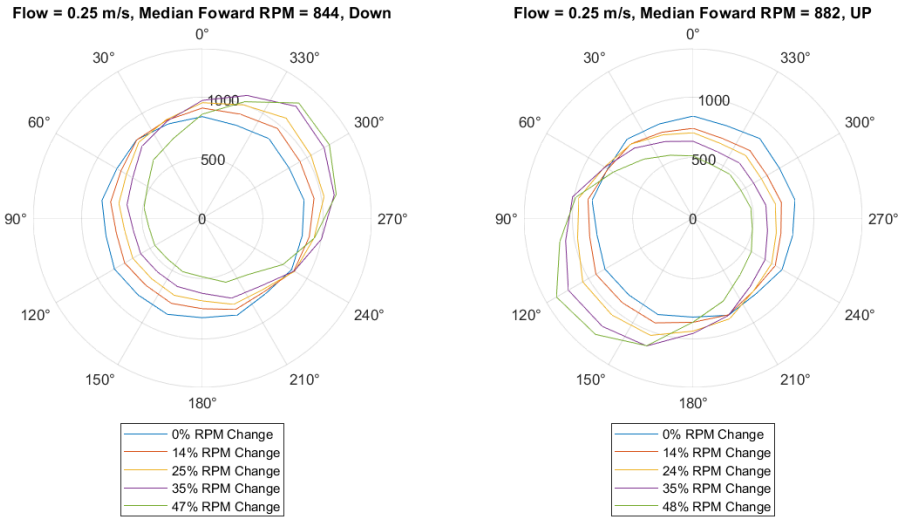

Figure 22. Polar plots of RPM as a function of angular position when generating maneuvering torques down(left) and up(right) at flow speed of 0.25 m/s

Figure 22 contains the polar figures for the RPM percent change as a function of angular position. The maximum RPM in elevator is up at 1,306 mean RPM. The minimum RPM in elevator is down at 445 mean RPM. At 0.25 m/s flow speed, thrust has an overall downward trend when generating a maneuvering torque down. When generating a maneuvering torque up, the thrust has a decrease to 14% RPM change. From there, thrust increases through 35% RPM change, then decreases at 48% RPM change. The change in pitch increases when elevating up and decreases when elevating down. The linear regression for change in pitch, has a slope of 0.0011 (N-m)/(%RPM Difference), an intercept of 0.0094 (N-m) and a R^2 value of 0.95.

Figure 24 shows the magnitudes of total torques with respect to % RPM Difference.

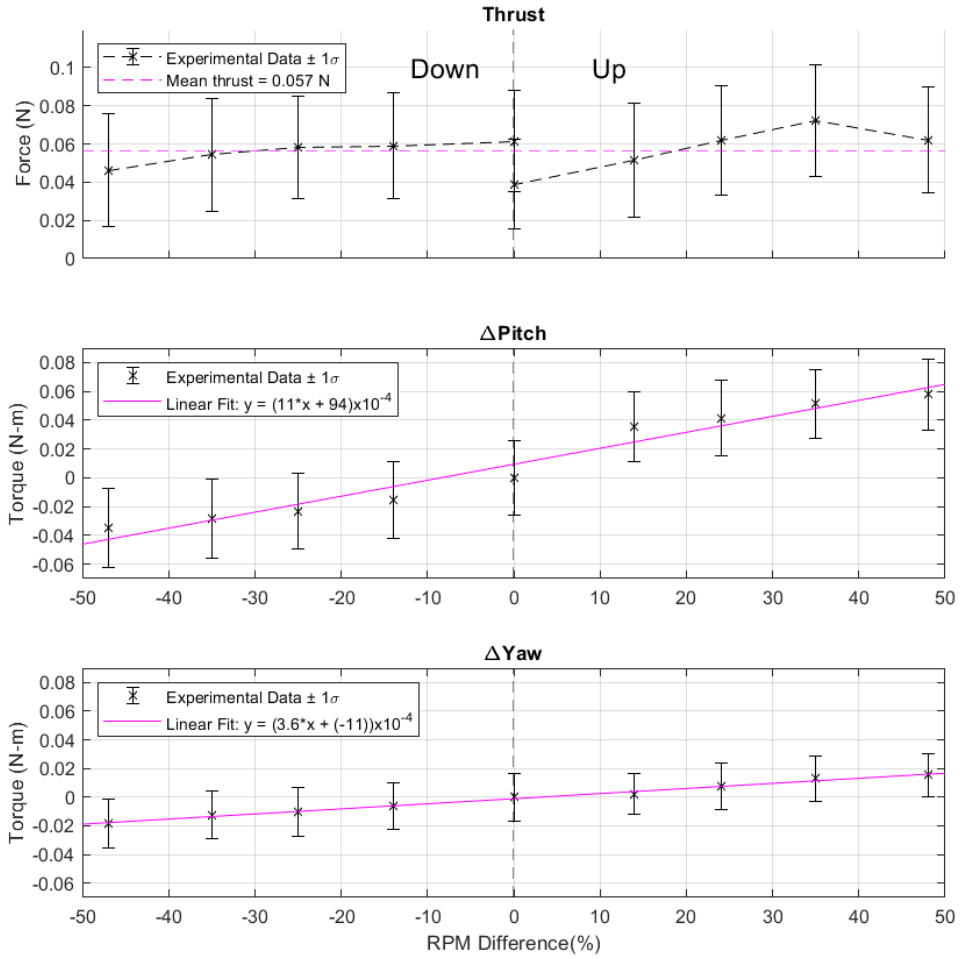

Figure 23. Thrust, change in pitch and change in yaw when generating a maneuvering torque up and down at flow speed of 0.25 m/s

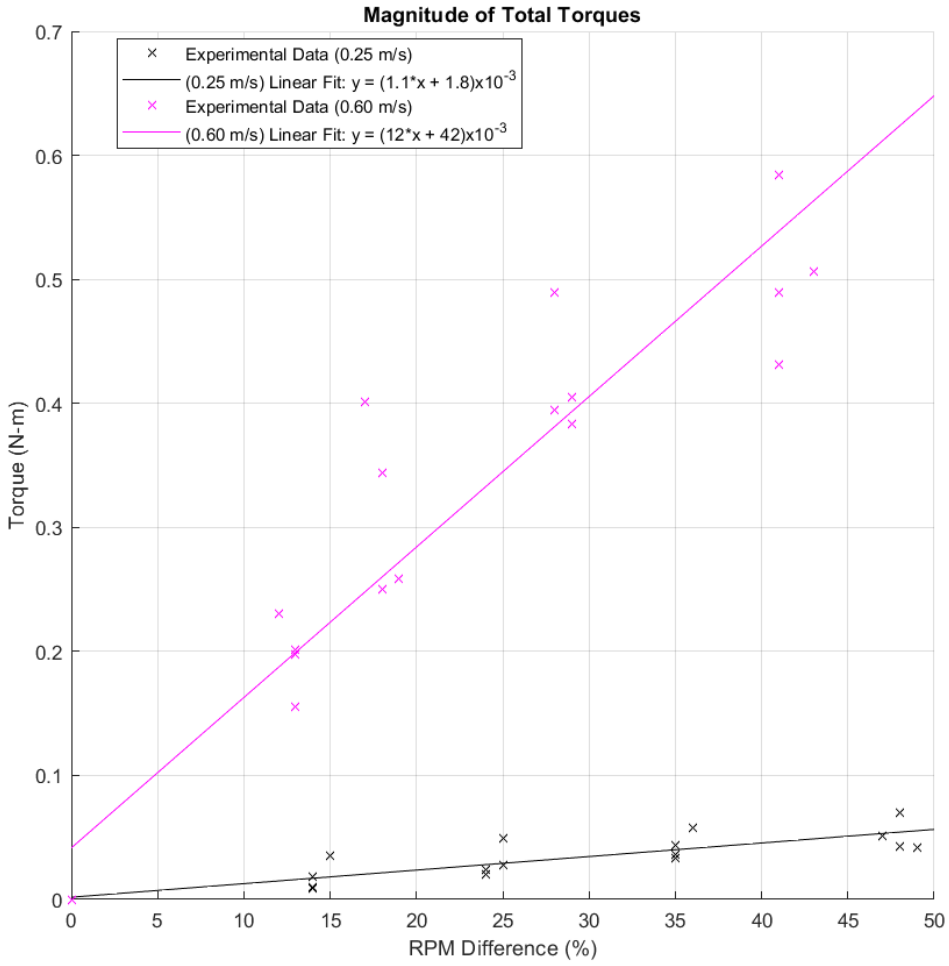

Figure 24. Combined magnitudes of change in pitch and yaw

CHAPTER 4

Discussion

For rudder actuation, there is a positive change in yaw when generating a starboard maneuvering torque as defined in the body frame. Further, the maximum magnitude for the pitch data is 47% of the maximum magnitude for the yaw data. When concerned with elevator actuation, there is a positive change in pitch for generating a maneuvering torque upward as defined in the body frame. The maximum magnitude for the change in yaw is 18% of the maximum magnitude from change in pitch data.Thrust values stayed within 32% of thrust at 0% RPM difference.

4.1 Effect of RPM difference on total magnitude of maneuvering torque

Figure 24 shows a clear linear relationship between %RPM Difference and torque. There is more variability in the torque values at higher speeds than at lower speeds. Though understanding the direction of torque generation is not completely clear, there is confidence in the predictability in overall torque generation. The trend of the generated torque values are expected. Increasing the % RPM delta causes an increase in the total magnitude of maneuvering torque. The total magnitude of maneuvering torque increases at a faster rate at higher flow speeds. This suggests an asymmetrical propulsion system on a mission in open water has more tighter turning capabilities at faster speeds than at slower speeds.

4.2 Uncertainty in propeller trajectory and impact on control of maneuvering torque produced

With regards to RPM, the accuracy of the instantaneous RPM values are unclear in relation to their angular displacement throughout a revolution. The RPM is expected to peak at 0°, 90°, 180° and 270° when generating maneuvering torques down, starboard, up, and port respectively. The maximum RPM values occur 40-50° from the expected position. The unexpected results with maneuvering torque direction as well as the angular position of peak instantaneous RPM values could be a result of incorrect reporting of propeller position from the onboard electronics or could be effects from the dynamics of the wake. If the onboard electronics are correct in reporting propeller trajectory, there would be discrepancies between commanded steering and actual steering angle. Addressing this potential discrepancy could create a situation where commanding rudder actuation creates no pitch actuation. If the onboard electronics are incorrect in reporting propeller trajectory, this could mean any maneuvering torques generated in an unintended direction resulted from wake effects.

CHAPTER 5

Conclusion and Future Work

Overall, the relationship between maneuvering torque and % RPM difference is expected. As the % RPM difference increases the magnitude of the change in maneuvering torque increases as well. It is believed that the apparatus and processes developed in this thesis are capable of accurately measuring maneuvering torques acting on the body of the vehicle. Though the embedded electronics on the vehicle generate a maneuvering torque in unexpected directions, generating some yaw actuation when intending to generate pitch actuation and vice-versa, the linear relationship between overall maneuvering torque magnitude and % RPM difference shows control over the total maneuvering torque generated.

The next steps in experimentation are to determine the instantaneous RPM of the propeller with respect to the angular position of the blade. This can be done through running a strobe light at the same frequency of the mean RPM of the propeller while capturing this process on a high speed camera. In order to characterize the angular kinematics of the propeller the exact instantaneous trajectory of the propeller must be known. This will also determine the accuracy of the RPM data output from the electronics onboard the vehicle.

The following step is to map the wake profile created by the propeller. This can be done through particle image velocimetry (PIV). An understanding of the trajectory will lead to an understanding of the wake generation when the wake profile is mapped and visualized. These additional data will provide insight into the dynamometry data of the vehicle.

APPENDIX

Appendix A: Forces in y and z axes

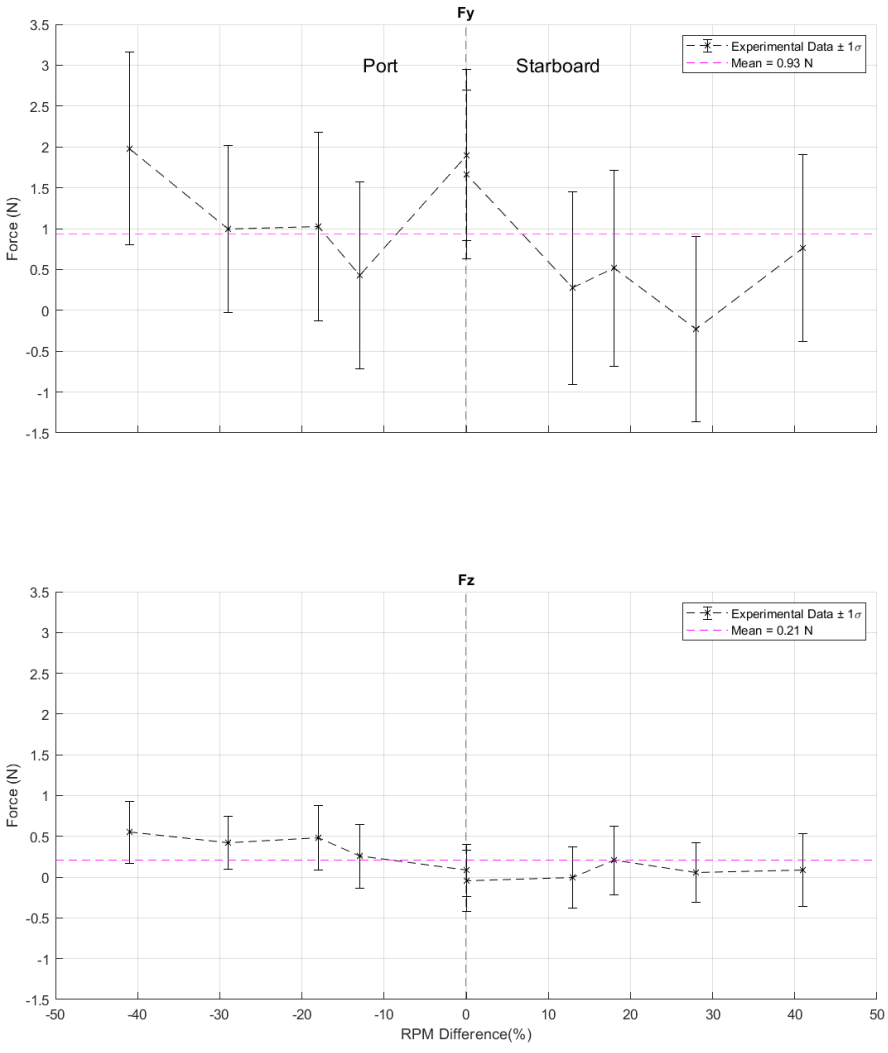

Figure A.1. Forces in y and z, rudder actuation at 0.60 m/s flow speed

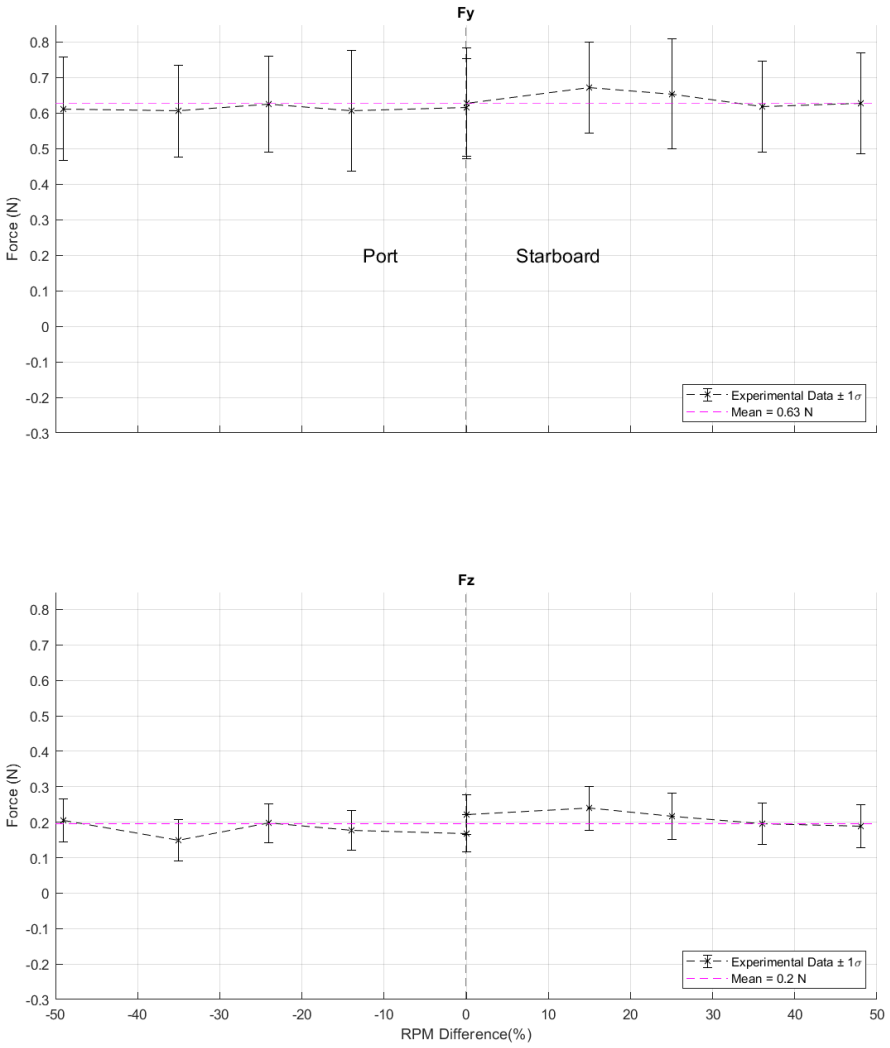

Figure A.2. Forces in y and z, rudder actuation at 0.25 m/s flow speed

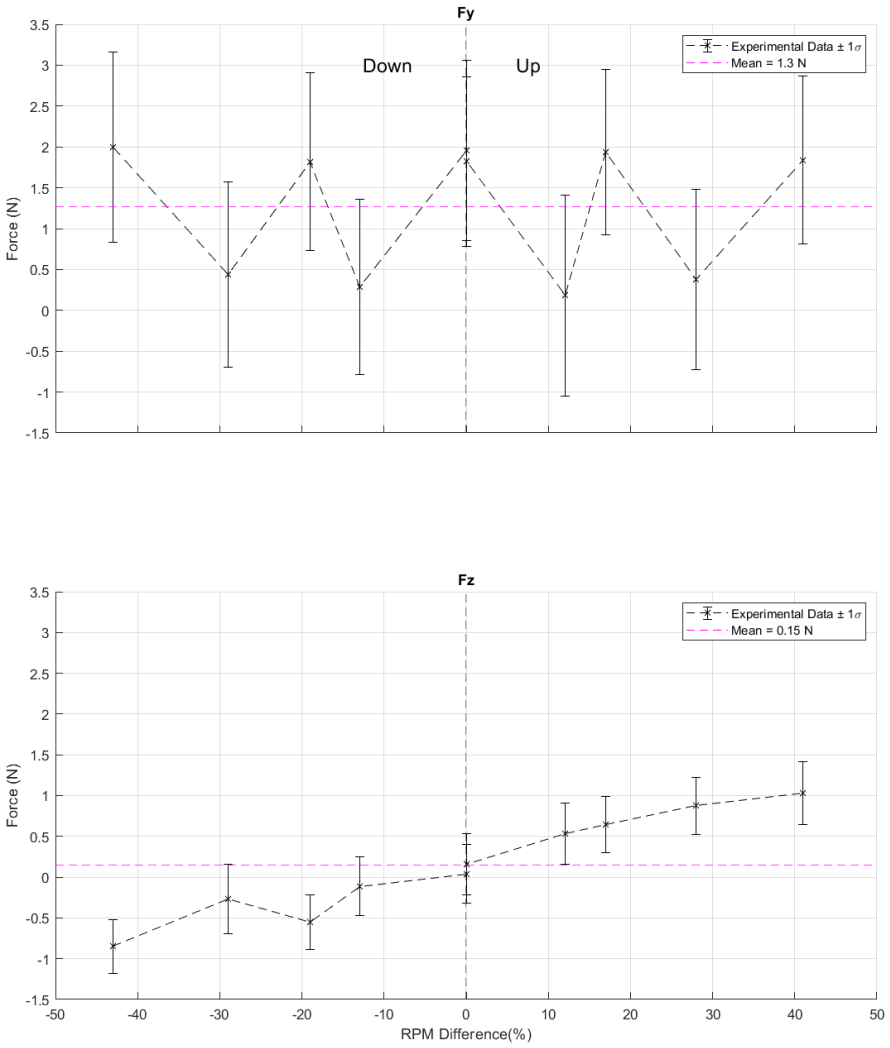

Figure A.3. Forces in y and z, rudder actuation at 0.60 m/s flow speed

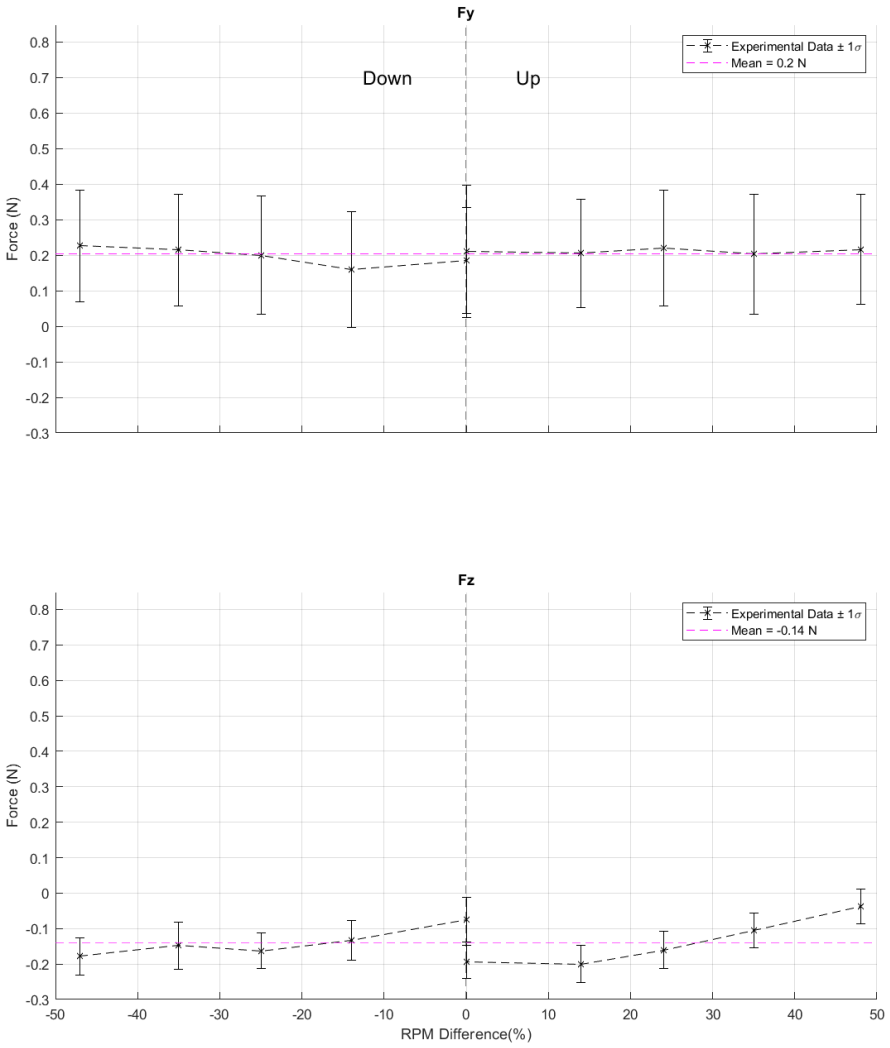

Figure A.4. Forces in y and z, rudder actuation at 0.25 m/s flow speed

BIBLIOGRAPHY

[1] National Geographic Society, “Ocean,” *National Geographic*. 20-May-2022.

[2] B. Phillips, J. Allder, G. Bolan, R. Nagle, A. Redington, T. Hellebrekers, J. Borden, N. Pawlenko, and S. Licht, “Additive manufacturing aboard a moving vessel at sea using passively stabilized stereolithography (SLA) 3D printing,” *Additive Manufacturing*, vol. 31, p. 100969, 2020.

[3] B. T. Phillips, S. Licht, K. S. Haiat, J. Bonney, J. Allder, N. Chaloux, R. Shomberg, and T. J. Noyes, “Deepi: A miniaturized, robust, and economical camera and computer system for deep-sea exploration,” *Deep Sea Research Part I: Oceanographic Research Papers*, vol. 153, p. 103136, 2019.

[4] K. D. von Ellenrieder, H. C. Henninger, and S. Licht, “Dynamic modelling and control of a portable USV for bathymetric survey,” *Global Oceans 2020: Singapore – U.S. Gulf Coast*, 2020.

[5] R. Gilboa, “Design and system identification of a low-cost USV for coastal observation.” University of Rhode Island, Narragansett, RI, 2022.

[6] P. V. Stefanoudis, W. Y. Licuanan, T. H. Morrison, S. Talma, J. Veitayaki, and L. C. Woodall, “Turning the tide of Parachute Science,” *Current Biology*, vol. 31, no. 4, 2021.

[7] J. Kaeli, R. Littlefield, and F. Jaffre, “Asymmetric propulsion: Thrust and maneuverability from a single degree of freedom,” *OCEANS 2019 MTS/IEEE SEATTLE*, 2019.

[8] R. H. Littlefield, F. Jaffre, and J. W. Kaeli, “AUV propulsion and maneuvering by means of asymmetric thrust,” *2018 IEEE/OES Autonomous Underwater Vehicle Workshop (AUV)*, 2018.

[9] R. B. Carelli, “Use of an asymmetric propeller for unmanned underwater vehicles,” dissertation, Massachusetts Institute of Technology, Cambridge, MA, 2019.

[10] Ellenrieder, Karl Dietrich von. *Control of Marine Vehicles*. Springer, 2021.